Arabidopsis uses a molecular grounding mechanism and a biophysical circuit breaker to limit floral abscission signaling

Isaiah W. Taylor*, O. Rahul Patharkar, Medhavinee Mijar, Che-Wei Hsu, John Baer, Chad E. Niederhuth, Uwe Ohler, Philip N. Benfey[1], John C. Walker[1]*

(1) These authors co-supervised this work

*corresponding authors

Isaiah W. Taylor: iwtwb8@gmail.com

John C. Walker: walkerj@missouri.edu

Abstract

Abscission is the programmed separation of plant organs. It is widespread in the plant kingdom with important functions in development and environmental response. In Arabidopsis, abscission of floral organs (sepals, petals, and stamens) is controlled by two receptor-like protein kinases HAESA (HAE) and HAESA LIKE-2 (HSL2), which orchestrate the programmed dissolution of the abscission zone connecting floral organs to the developing fruit. In this work, we use single-cell RNA-Sequencing to characterize the core *HAE/HSL2* abscission gene expression program. We identify the *MAP KINASE PHOSPHATASE-1/MKP1* gene as a negative regulator of this pathway. MKP1 acts prior to activation of HAE/HSL2 signaling to establish a signaling threshold required for the initiation of abscission. By analogy to electrical circuit control, we liken MKP1 to a molecular grounding mechanism that dissipates errant pathway activation absent HAE/HSL2 signaling. Furthermore, we use single-cell data to identify genes expressed in two sub-populations of abscission zone cells: those proximal and those distal to the plane of separation. We identify *INFLORESCENCE DEFICIENT IN ABSCISSION/IDA*, encoding the activating ligand of HAE/HSL2, as one of the mRNAs most highly enriched in distal abscission zone cells at the base of the abscising organs. We show how this expression pattern forms a biophysical circuit breaker whereby, when the organ is shed, the source of the IDA peptide is removed, leading to cessation of HAE/HSL2 signaling. Overall, this work provides insight into the multiple control mechanisms acting on the abscission-signaling pathway.

Introduction

Abscission is a ubiquitous process occurring at multiple stages of the plant life cycle. Shedding of leaves in the autumn and fruit after ripening are common examples, as is shedding of organs after damage or infection[1–3]. Historically, selection for grass varieties with defects in seed abscission (also known as shattering) dramatically increased the efficiency of harvest and is considered one of the critical steps in domestication[4]. Controlling abscission today is still of agricultural and horticultural relevance in a wide range of species[5–8].

In the genomics era, abscission of Arabidopsis floral organs is among the best studied systems[9]. In particular, Arabidopsis floral abscission has been shown to be regulated by ethylene, auxin, and their interaction[10–12], with additional contributions from jasmonic acid and abscisic acid signaling[13,14]. In Arabidopsis, the site of floral abscission, known as the abscission zone (AZ), is lignified on the distal

38 margin to create a well-defined separation plane[15]. During abscission, the middle lamella (the pectin-rich
39 substance adhering adjacent cells) is degraded enzymatically before the organs detach[16].

40 Abscission in Arabidopsis is regulated by two related leucine-rich repeat receptor-like protein kinases
41 (LRR-RLKs) HAESA/HAE and HAESA LIKE-2/HSL2. The double mutant *hae hsl2* fails to shed its floral
42 organs[17–19]. Several components of the *HAE/HSL2* signaling pathway regulating abscission have been
43 discovered. In particular, HAE and HSL2 cooperate with members of the SOMATIC EMBRYOGENSIS
44 RECEPTOR KINASE/SERK family of co-receptor LRR-RLKs to bind the proteolytic-processing derived
45 INFLORESCENCE DEFICIENT IN ABSCISSION/IDA peptide, which activates a MAP kinase cascade[18,20–22].
46 MAPK signaling triggers expression of downstream abscission genes involved in pectin degradation, cell
47 wall remodeling, and, ultimately, separation of the abscising organs[18,23–27]. A number of transcription
48 factors have been implicated in regulating AZ development and abscission signaling [14,28–31]. It has been
49 shown that *Nicotiana* lines with silenced *HAE* and *IDA* orthologs exhibit reduced perianth abscission[32],
50 and expression of both citrus ad litchi orthologs of *IDA* can complement the abscission-deficient *ida*
51 mutant phenotype in Arabidopsis[33,34]. We have also demonstrated abscission of Arabidopsis cauline
52 leaves upon water stress or pathogen infection is under similar genetic control as floral abscission[35,36].
53 These results indicate the knowledge of the specific components of the *HAE/HSL2* pathway will inform
54 regulation of abscission in multiple systems across multiple species.

55 While knowledge of positive regulators of Arabidopsis abscission signaling has been increasing in recent
56 years, we know comparatively little about negative regulation of this process. This is a notable gap
57 because plants must tightly control abscission signaling to avoid negative fitness consequences such as
58 premature shedding of stamens and developing fruit. Moreover, prolonged abscission signaling could
59 lead to wound formation, posing the risk of infection and desiccation. Among the negative genetic
60 regulators we know include AGL transcription factors (such as AGL15 that has been shown to bind and
61 negatively regulate the *HAE* promoter, repression of which is a component of a positive feedback loop),
62 as well as the pseudo-kinase BIR1 (implicated in negatively regulating a SERK-SOBIR1 mediated signaling
63 cascade)[20,26,37–39].

64 In this work, we provide insight into how the abscission pathway is maintained at a low basal activity
65 prior to abscission activation. We also describe an abscission termination mechanism that highlights
66 how plants have evolved an elegantly simple way to halt the abscission process. We began our work by
67 hypothesizing that assessing the transcriptional output of the *HAE/HSL2* pathway at the single-cell level
68 could help us answer questions surrounding the dynamics of how abscission is orchestrated, and how
69 the cell types within the AZ coordinate in this orchestration. This line of investigation led to the
70 characterization of a mutant in a phosphatase gene that we show negatively regulates basal signaling
71 prior to abscission pathway activation. Second, we establish how a spatial gradient in *IDA* expression
72 contributes to limiting HAE/HSL2 signaling to the time when organs are attached. In essence, we
73 demonstrate that IDA is a key switch that the plant has localized to the AZ cells on the abscising organ,
74 ensuring that the trigger for the abscission pathway is physically removed from the plant once abscission
75 has occurred. This creates a virtually infallible way of terminating abscission signaling, thus eliminating
76 the potential hazards of uncontrolled pathway activation.

77 **Results**

78 **Single-cell RNA-Sequencing identifies floral abscission zone cells**

The genes encoding HAE and HSL2 are required for floral organ abscission in Arabidopsis [Figure 1A]. In order to characterize transcriptional outputs of *HAE/HSL2* signaling, we developed a flower receptacle protoplasting method (Materials and Methods) and used it to perform scRNA-Seq on stage 15 floral receptacles of WT and *hae hsl2* (2 replicates each) [Fig. 1B]. Stage 15 is the time when abscission signaling has been initiated, but WT and *hae/hsl2* are still morphologically comparable. We also profiled 2 replicates each of FACS sorted cells derived from *hae hsl2* + *HAEpr::HAE-YFP* (complemented) and kinase dead *hae hsl2* + *HAEpr::HAE-K711E-YFP* (non-complemented) receptacles to further enrich for AZ cells from phenotypically wild-type and mutant plants, respectively [Figures 1C and 1D] (Materials and Methods). In total, we obtained data for 4 WT/complemented (hereafter "WT"*)* and 4 mutant/non-complemented (hereafter "*hae hsl2*") replicate samples each, granting us robust statistical power to identify genes regulated by *HAE/HSL2* signaling (Supplemental Table 1 and Supplemental Figure 1 for sample sequencing metrics). After preprocessing and filtering low quality cells, we integrated all cells using Seurat[40], excluding genes whose expression was altered in a separate receptacle protoplast bulk RNA-Seq experiment (Materials and Methods). We used Louvain clustering to identify transcriptionally similar groups of cells and embedded them in a 2-dimensional Uniform Manifold Approximation and Projection (UMAP) [Figure 2A, top panel]. Next, we plotted WT cells on the UMAP expressing known markers of the AZ: *HAE* and the pectin degrading enzyme-encoding genes *QUARTET2/QRT2* and *POLYGALACTURONASE AZ OF A. THALIANA/PGAZAT* [Figure 2A, bottom panel]. A compact group of cells was apparent in the UMAP expressing all three AZ markers (Figure 1A, lower panels). These cells, numbering 869 out of a total of 16169 profiled WT cells (5.4%), grouped together across a wide range of Louvain clustering resolutions [Figure 2A, pink border, Supplemental Figure 2]. Thus, this group of cells appears to represent the AZ, which is transcriptionally identifiable and highly distinct from other cell types in the receptacle.

To confirm the identity of the putative AZ, we took several approaches. First, we sorted *HAE-YFP* expressing cells and generated and sequenced bulk RNA-Seq libraries (Materials and Methods, Supplemental Table 2). We then calculated cluster-wise Spearman correlation between this dataset and pseudo-bulked data of each of the identified clusters from the single-cell experiment. The putative AZ cluster displayed the highest correlation, consistent with the hypothesis that it represents the AZ [Figure 2B, top panel]. Similarly, we used published bulk RNA-Seq data from FACS sorted *QRT2*-expressing stage 16 AZ cells to perform an identical correlation analysis and found that, again, this cluster displayed the highest correlation [Figure 2B, bottom panel, Supplemental Tables 3 and 4][15]. Next, we identified genes enriched in the putative AZ cluster (not previously known to be specific to the AZ) and generated promoter::fluorescent reporter lines [Figure 2C]. All four reporters displayed highly specific expression in the AZ cells, indicating this cluster represents the AZ.

To characterize the biology of the putative AZ, we identified AZ enriched genes using Seurat (Materials and Methods, Supplemental Tables 5 and 6). Analysis of Gene Ontology (GO) terms found enrichment of genes associated with middle lamella degradation and cell wall remodeling (pectin catabolic process, polysaccharide catabolic process, galacturonan metabolic process, etc.) [Figure 2D]. Additionally, there were terms associated with extracellular barrier formation such as phenylpropanoid biosynthesis, the major pathway leading to lignin formation, which has been shown to play an important role in the delineation of the AZ in both Arabidopsis and rice[15,41]. Terms related to Fatty-acyl-CoA metabolism are associated with genes involved in cutin biosynthesis, a waxy substance deposited on the scar of newly

121 differentiated epidermal cells after abscission has occurred[15]. Overall, these terms are highly consistent
122 the AZ being a site of focused cell wall disassembly and barrier formation.

123 While not the focus of this study, we were also curious if we could identify other non-AZ cell types
124 present in the receptacle. Indeed, many genes associated with specific cell types from Arabidopsis leaf
125 scRNA-Seq data were present in restricted clusters in our data[42], allowing us to make tentative
126 assignments of epidermis, mesophyll, guard cells, etc [Supplemental Figure 3A-C]. This suggests that
127 floral organs, as modified leaves, retain some of the gene expression patterns of their homologous
128 organs. There were also clusters that did not express known leaf markers [Supplemental Figure 3B],
129 likely representing less characterized, flower-specific cell types. For example, we identified a large group
130 of cells expressing AT3G01420, an alpha dioxygenase encoding-gene previously shown to be highly
131 enriched in bulk RNA-Seq of developing siliques[43], suggesting that there are uncharacterized flower-
132 specific cell types [Supplemental Figure 3D].

133 **The *hae hsl2* mutant exhibits a reduction in expression of genes associated with core abscission zone**
134 **signatures**

135 We next examined the scRNA-Seq data to characterize gene expression differences between *hae hsl2*
136 and WT. Plotting mutant cells by UMAP indicates a similar spectrum of cell types as WT [Figure 3A], with
137 a similar proportion of putative AZ cells numbering 964 out of 24497 profiled mutant cells (3.9%). To
138 identify differentially expressed genes (DEGs), we performed pseudo-bulk analysis comparing WT to *hae*
139 *hsl2* using edgeR[44]. This analysis revealed 302 genes with lower expression and 274 with higher
140 expression in the double mutant as compared to WT [Supplemental Table 7].

141 GO term enrichment of genes with reduced expression in *hae hsl2* AZ was consistent with known
142 biology of abscission, including terms related to pectin degradation and cell wall remodeling [Figure 3B,
143 Materials and Methods]. Terms associated with suberin deposition are likely to reflect biosynthesis of
144 cutin, a related wax compound with similar biosynthesis, which has been shown to accumulate in
145 Arabidopsis floral AZs[15]. For visualization, we plotted the expression levels of a number of known and
146 novel *HAE/HSL2* regulated genes [Figure 3C]. Overall, these results are consistent with the role of
147 *HAE/HSL2* as central regulators of genes required for breakdown and remodeling of the cell wall during
148 abscission. Interestingly, GO term analysis of genes with higher expression in *hae hsl2* did not reveal
149 such clearly biologically interpretable signals and was enriched in terms associated with defense and
150 hypoxia responses [Supplemental Figure 4]. This suggests there may be novel molecular pathways
151 repressed by *HAE/HSL2* that can be interrogated in future work.

152 ***hae hsl2* suppressor mutants partially restore the abscission zone gene expression signature**

153 Having identified a core set of genes regulated by *HAE/HSL2* specifically in the AZ, we set out to
154 characterize this signaling pathway in two novel *hae hsl2* partial suppressor mutants isolated from a
155 previously described *hae hsl2* T-DNA suppressor screen[26]. These mutants, which we named *fal-3* and *fal-*
156 *7* for *facilitated abscission locus,* display a cool-temperature-enhanced suppression of the *hae/hsl2*
157 phenotype when grown at 16° [Fig 4A]. This can be quantified by measuring the force required to
158 remove petals of stage 16 flowers using a previously described petal break-strength assay [Fig 4B][45].

159 Based on the partial suppression phenotype, we hypothesized that gene expression changes in *hae hsl2*
160 would be partially reversed in the *hae hsl2 fal-3* and *hae hsl2 fal-7* suppressors. To test this hypothesis,

161 we performed stage 15 receptacle bulk RNA-seq of plants grown at 16° comparing WT, *hae hsl2*, *hae*
162 *hsl2 fal-3* and *hae hsl2 fal-7* and examined the expression of 67 genes that were reduced both in
163 *hae/hsl2* in the AZ in our single-cell data while also exhibiting a reduction in previously published
164 receptacle bulk RNA-Seq experiments comparing WT and *hae/hsl2* [Supplemental Tables 8 and 9][26,27].
165 Thus, these genes represent an AZ-specific, validated set of genes regulated by *HAE/HSL2* identifiable
166 from bulk analysis [Supplemental Figure 5]. Indeed, in *hae hsl2 fal-3* and *hae hsl2 fal-7,* most of these
167 genes show an intermediate level of expression between WT and *hae hsl2* [Figure 4C]. To perform a
168 single composite statistical test, we used Parametric Analysis of Gene Expression/PAGE, which averages
169 expression of a set of genes on a log scale and uses the resulting approximate normality to perform
170 comparisons[46] (Materials and Methods). Consistent with the hypothesis that the suppressors have
171 partial reversion of the abscission gene expression program, the average log2(FC) levels for both *hae*
172 *hsl2 fal-3* and *hae hsl2 fal-7* are intermediate between WT and *hae hsl2* [Figure4D]. These results
173 confirm the partial suppression phenotype is due to partial *HAE/HSL2* pathway activation in these
174 mutants.

175 **Mutation of *MAP KINASE PHOSPHATASE-1/MKP1* underlies the *hae hsl2 fal* suppression phenotype**

176 To identify the causative mutations in *fal-3* and *fal-7* we performed complementation crosses, which
177 indicated that *fal-3* and *fal-7* are allelic, recessive mutations [Figure 4E]. To identify the underlying
178 mutations, we performed TAIL-PCR and found *fal-7* harbors a T-DNA insertion in the first exon of *MAP*
179 *KINASE PHOSPHATASE-1/MKP1,* a gene encoding a phosphatase known to negatively regulate MPK3 and
180 MPK6 during biotic and abiotic stress signaling in a cool-temperature enhanced manner [Figure 4F][47,48].
181 Because MPK3/6 are also involved in abscission signaling[18], and because the effect of *fal-3* and *fal-7* is
182 cold-enhanced, *MKP1* became a very strong candidate gene. In *fal-3*, we identified a SNP causing a
183 premature stop codon in the first exon of *MKP1* leading to truncation of nearly half the protein [Figure
184 4F]. In addition, segregation analysis of a back-cross population of *hae hsl2 x hae hsl2 fal-7* indicated the
185 *hae hsl2* suppression effect is linked to the insertion in *MKP1* [Supplemental Figure 6] confirming that
186 the phenotype of *fal-3* and *fal-7* is due to mutation of *MKP1.*

187 These results together indicate MKP1 is a negative regulator of abscission that buffers low levels of basal
188 signaling which could otherwise induce abscission in the absence of HAE/HSL2 activation. This molecular
189 thresholding mechanism is likely critical to prevent errant signal amplification of background noise and
190 to ensure coherent activation of downstream signaling across the AZ. By analogy, this resembles the
191 safety mechanism of grounding in electrical systems where the neutral and ground wires in the main
192 electrical panel are bonded to set neutral voltage to the reference ground value of zero. This allows
193 unwanted energy a dissipation path, preventing unwanted voltage noise on inactive circuits. In a similar
194 fashion, MKP1 eliminates spurious MAPK phosphorylation that could lead to premature pathway
195 activation prior to abscission signal induction.

196 **Single-cell RNA-Seq identifies spatial domains of the abscission zone**

197 While the above analysis relied on pseudo-bulk measurements of gene expression across the entire AZ,
198 we were next interested to explore whether we could potentially obtain more fine-grained information
199 on the function of distinct cell populations within the AZ. An important report from Lee et al[15] provided
200 a detailed examination of the spatial organization of the AZ, identifying a differentiated group of cells on

201 the distal side at the base of the abscising organ (termed *secession cells*) and a distinct group on the
202 proximal side of the abscising organ (termed *residuum cells*) [Figure 5A]. Functionally, secession cells
203 form a lignin "brace," which is thought to focus the enzymatic activity of secreted hydrolases to the
204 middle lamella of the fracture plane at the site of abscission, while also creating a rigid frame which
205 detaches once sufficient weakening of the fracture plane has occurred.

206 This process had previously been detailed in stage 16 flowers, just as abscission is occurring[15]. We
207 hypothesized we may be able to detect evidence of the differentiation process at stage 15 from our
208 data. Interestingly, when performing low resolution Louvain clustering of WT AZ cells and embedding in
209 UMAP space, two groups of cells emerge [Figure 5B, left panel]. We tested the hypothesis that these
210 cells represent secession and residuum cells by performing cluster-wise Spearman correlation analysis
211 with previously published bulk RNA-Seq data derived from sorted secession cells and, separately, sorted
212 residuum cells[15]. Consistent with our hypothesis, we observed a strong association of one of the two
213 clusters of cells with secession bulk data [Figure 5B, middle panel] and strong association of the second
214 group of cells with residuum bulk data [Figure 5B, right panel].

215 To validate the hypothesis that these cell clusters represent distinct sides of the AZ, we performed a
216 pseudo-bulk differential enrichment analysis to identify genes enriched in the putative secession and
217 residuum cells. We identified 306 and 540 genes displaying evidence of enrichment in these cell types,
218 respectively [Supplemental Table 10]. GO term enrichment analysis of the secession cell-associated
219 genes in revealed modest enrichment of pathways related to phenylpropanoid biosynthesis [Figure 5C,
220 top panel]. Since one of the main functions of the phenylpropanoid pathway is lignin formation, this is
221 consistent with the idea that putative secession cells are in the early stages of forming a lignin brace. In
222 contrast, the genes associated with putative residuum cells are enriched in terms related to cellular
223 activity such as protein production [Figure 5C, lower panel]. This is consistent with classical observations
224 that AZ cells are sites of high levels of protein synthesis[49]. Interestingly, we performed a similar analysis
225 of putative secession and residuum cells in mutant samples, and we found evidence of significantly
226 fewer genes enriched in the mutant cell types, suggesting *HAE/HSL2* may drive cellular differentiation of
227 these two cell types within the AZ [Supplemental Figure 7 and Supplemental Table 11].

228 To provide final validation of the identification of AZ sub-types, we identified one gene, *AT5G57785*,
229 encoding a predicted mitochondrial protein of unknown function, as a gene highly enriched in the
230 putative residuum side of the AZ [Fig 5D]. Promoter::reporter analysis confirmed this expression
231 pattern, showing the gene is relatively low-expressed in secession cells, but highly expressed across the
232 residuum [Figure 5E, Supplemental Table 10]. In contrast, and intriguingly, we found one of the most
233 highly enriched genes in the putative secession cells is *IDA*, encoding the activating ligand of HAE/HSL2
234 [Figure 5F, Supplemental Table 10]. We confirmed this pattern by generating promoter::reporter lines,
235 demonstrating strong expression in secession cells and only patchy expression in residuum cells [Figure
236 5G]. These results confirm the ability of single-cell RNA-Seq to discriminate AZ sub-types.

237 **Localization of *IDA* expression to abscising organs terminates *HAE/HSL2* signaling after organ**
238 **separation**

239 Finally, we noted that it is interesting that while *IDA* is highly enriched on the secession side of the AZ,
240 other signaling components such as *HAE, HSL2,* and *MKP1* are detected at similar levels in both
241 residuum and secession cells [Supplemental Figure 8]. This specific enrichment of *IDA* in secession cells
242 suggested to us a potential elegant regulatory control mechanism. In this model, the soluble IDA peptide

243 is secreted by secession cells to activate signaling locally, at the site of organ attachment, while diffusing
244 across the secession-residuum boundary to activate signaling in residuum cells in trans. However, once
245 cell separation occurs, the source of the activating IDA ligand (i.e., the base of the abscising organ) is
246 physically detached from the plant, leading to signal attenuation.

247 One prediction of this model is that if *IDA* were mis-expressed in the residuum cells we might observe
248 some evidence of HAE pathway over-activation. To test this prediction, we expressed the *IDA* gene in
249 residuum cells by fusing it to the residuum specific *AT5G57785* promoter fragment characterized above.
250 Indeed, we observed plants displaying highly enlarged, disorganized AZs [Figure 5G]. This phenotype has
251 previously been observed in cases where the *IDA-HAE/HSL2* pathway is over-activated, for instance
252 through general over-expression of *IDA* or mis-expression of the activating TF *WRKY57* [18,19,30]. This result
253 indicates that localizing *IDA* on the secession side of the AZ ensures the clean and abrupt cessation of
254 signaling that occurs in WT after abscission has occurred. Importantly, we have previously shown over-
255 expression of *HAE* does not lead to such a pathway over-activation phenotype, instead yielding
256 phenotypically WT plants[50]. Thus, these results together demonstrate a novel mechanism by which the
257 physical removal of the source of IDA is likely the main signal attenuation mechanism to deactivate
258 signaling once abscising organs are shed. A diagram of the model of abscission signal control is shown in
259 Figure 6.

260 **Discussion**

261 This work highlights two important emergent properties of abscission signaling. First, the pathway must
262 be tightly regulated to prevent signaling absent inducing stimulus which might lead to premature
263 abscission (exemplified here by MKP1 maintaining basal signaling below a threshold level prior to
264 pathway activation). This could be necessary since the abscission pathway is forcefully activated by
265 positive feedback, placing the pathway under the control of a molecular hair trigger[20]. Second, activation
266 of the pathway should be restricted to the site of organ attachment and be turned off after abscission
267 has occurred. This avoids widespread and prolonged signaling leading to wounding. Our work shows
268 that during Arabidopsis floral abscission, this is accomplished by localizing the source of the inducing
269 signal IDA to the abscising organ. The ingeniously designed abscission switch constitutes a failsafe
270 biophysical circuit breaker that terminates a highly amplified abscission activation signal, along with the
271 potentially deleterious cellular processes that result from it. Diffusion of IDA peptide from source
272 secession cells establishes a gradient across both sides of the abscission zone that does not appear
273 necessary for abscission to take place. However, mis-expression of *IDA* in residuum cells, creating an
274 altered IDA gradient, results in malformed residuum abscission scars, demonstrating the regulatory logic
275 of restricting *IDA* expression to the AZ cells on the abscising organ. We propose both highlighted
276 mechanisms are likely general features of the regulation of abscission across species and organ types.

277 It is interesting to note that Thomas Edison invented the electrical circuit breaker in 1879 to prevent
278 fires arising from electrical short-circuits and overloading[51]. Nature appears to have solved a similar
279 problem over the course of millions of years of evolution of abscission in plants. Equipping abscission
280 signaling circuitry with both a physical circuit breaker to terminate the process and a noise reduction
281 mechanism, resembling electrical grounding, to keep the circuitry completely off when not needed,
282 illustrates how simple, yet ingenious and effective, plant signaling system design can be.

283 **Methods**

284 **Plant growth**

285 The *hae-3 hsl2-3* mutant was used in all experiments[52]. Wild type, *hae-3 hsl2-3, hae-3 hsl2-3*
286 *HAEpr::HAE-YFP, hae-3 hsl2-3 HAEpr::HAE-YFP K711E, hae-3 hsl2-3 fal-3,* and *hae-3 hsl2-3 fal-7* are all in
287 the Columbia background. The *fal* suppressor mutants also contain *erecta* and *glabrous* mutations in
288 order to phenotypically differentiate contaminating wild-type seeds from mutants in the *hae hsl2*
289 suppressor screen[26]. Plants were grown in a 16-hour light cycle at either 22° or 16°, except for the
290 breakstrength experiments which were conducted at 23° and 16°. Plants were grown in peat
291 moss/vermiculite potting soil and fertilized every 3 weeks with ½ strength Miracle-Gro (Scotts Miracle-
292 Gro Company).

293 **Protoplasting and FACS**

294 For each protoplast sample, we isolated approximately 20 1 mm sections of stage 15 floral receptacles
295 of plants approximately 2 weeks post-bolting, in a similar manner as our previous work[26,53]. For
296 protoplasting, we employed the isolation method of Evrard et al, developed for rice roots, with minor
297 modifications[54]. In brief, we prepared digest solution as follows: per 30 mls we added 400 mM mannitol
298 (2.2 g), 20 mM MES hydrate (117 mg), 20 mM KCl (600 µL of 1 M KCl), after which the pH was adjusted
299 to 5.7 with KOH. We would typically make 500 mls of this solution, filter sterilize, and store at 4° for
300 several months. On the day of protoplasting, per 30 mls, we added 1.25% Cellulase R10 (375 mg), 1.25%
301 Cellulase RS (375 mg), 0.3% Macerozyme R10 (90 mg), 0.12% Pectolyase-Y23 (36 mg) and heated 10 min
302 in 60° water bath before cooling to room temperature (all digest enzymes purchased from Duchefa
303 Biochemie except Pectolyase-Y23, which was purchased from MP Biomedicals). Finally we added 10 mM
304 CaCl2 (300 µL of 1 M CaCl2), 0.1% BSA (30 mg), and 5.38 µL of β-mercaptoethanol. We sliced the
305 receptacles into quarters under a dissecting scope on 4% agarose plates with a fine micro-scalpel #715
306 (Feather), used forceps to transfer into 5 mls of digest solution in small petri dishes, and vacuum
307 infiltrated for 7 minutes at -25 inHg in a dome desiccator. We digested the tissue for 2.25 hours at 80
308 RPM on a rotary platform shaker at 25°, using fine forceps and micro-scalpel to additionally slice the
309 softened tissue at around 1.5 hours. We next filtered the cells twice through 40 um filters, spun for 5
310 minutes at 500 x g in a swinging bucket rotor in 5 ml sorting tubes, and rinsed twice with wash buffer
311 (digest buffer with no enzymes). Between washes we spun cells for 3 minutes at 500 x g. Finally, we
312 resuspended cells in wash buffer. It should be noted that it is now recognized calcium in the
313 resuspension buffer reduces the efficiency of reverse transcription[55,56], so it is recommended that for
314 follow-up studies, at least in the final resuspension step, calcium be omitted[56]. For receptacle single-cell
315 samples, cells were counted on a hemacytometer C-chip (SKC, Inc.) and the concentration adjusted to
316 1000 cells/µl (total yield ranged from approximately 50,000-100,000 cells). For sorted samples, cells
317 were prepared the same manner and sorted for YFP+ on a BD Diva cell-sorter into either excess wash
318 buffer (for single-cell samples) or directly into RNA-Later for bulk samples. Single-cell sorted samples
319 were then spun down and resuspended in 15 µl wash buffer. We took 2.5 µl of cells for dilution and
320 counting on a hemacytometer C-chip. Final yield for sorted samples was between 400-3000 cells, all of
321 which were run on a Chromium chip.

322 **scRNA-Seq library generation**

323 We used the 10x Genomics v3 3' Single-cell RNA-Seq kit for all samples. For the receptacle WT and *hae*
324 *hsl2* samples we followed the manufacturer's protocol, loading 16,000 cells per sample for a target
325 capture of 10,000 single cells. For sorted samples, we divided a single reaction into four 25 µl reactions

326 and ran on four lanes of a single chip. For sorted sample library preparation, we reduced the volume of
327 all reagents only by ½, which was enabled by excess reagents accumulated due to prior emulsion failures
328 (although we expect miniaturization to ¼-scale library preparations would be feasible). Raw reads have
329 been deposited at the Sequence Read Archive under BioProject PRJNA857332.

330 **scRNA-Seq library sequencing and preprocessing**

331 Unless otherwise noted, all analyses were performed in R 3.6.3 and are included, along with the output
332 of sessionInfo(), as Jupyter Notebooks in the Supplemental Code. We used our previously published
333 scKB procedure to align and produce count matrices for downstream analysis[57]. This pipeline uses
334 kallisto, bustools, busparse, and BSgenome[58–61] to align and quantify counts to the Arabidopsis TAIR10
335 genome. The following analyses are recorded in Notebook 1: For samples WT and *hae hsl2* receptacle
336 samples #1 we had performed species-mixed experiments containing rice and Arabidopsis cells, so we
337 aligned to a concatenated rice-Arabidopsis MSU7/TAIR10 genome using a combined gff file and retained
338 only reads mapping to Arabidopsis[50,52]. We pooled reads mapping to spliced and unspliced transcripts in
339 order to make a single matrix of gene expression values. We next ran EmptyDrops[63] in order to identify
340 putative empty droplets containing no cells with "ignore" parameter = 500 and "lower" parameter =
341 300. We then constructed Seurat objects with the expression matrices. We finally used doubletFinder[64]
342 to identify putative doublets using the approximate doublet rate employed by 10X as .004/500 * #
343 loaded cells. The resulting Seurat objects were used for downstream analysis. Our estimated number of
344 recovered cells after all these steps are: WT receptacle #1: 7509 cells, WT receptacle #2: 7571 cells, WT
345 sorted #1: 878 cells, WT sorted #2: 211 cells, *hae hsl2* receptacle #1: 14492 cells, *hae hsl2* receptacle #2:
346 7578 cells, *hae hsl2* sorted #1: 1302 cells, *hae hsl2* sorted #2: 1125 cells.

347 **Exploratory analysis of scRNA-Seq data and identification of the AZ**

348 Sample integration (Notebook 2) was performed by running SCTransform on each sample before
349 integrating, excluding mitochondrial genes, plastid genes, and genes altered by protoplasting (defined as
350 those with absolute value of log2(FC) > 1) [Supplemental Table 12]. We performed PCA, constructed a
351 shared nearest neighbor graph, and identified clusters using the SLM algorithm. Visualization was
352 performed by UMAP embedding.

353 Identification of the AZ (Notebook 3) was performed by first plotting *HAE*, *QRT2*, and *PGAZAT* in WT cells
354 of the UMAP embedding with the "min" parameter set to .5. We next calculated the pseudobulk
355 expression profile for all clusters identified at resolution .75 by summing all counts for each gene. We
356 next calculated Spearman correlation with bulk sorted *HAE+* and *QRT2+* RNA-Seq data. The *HAE* data
357 (Supplemental Table 2) was Lexogen Quant-seq 3' and consequently is directly convertible to Transcripts
358 per Million (TPM) making it comparable to 3' RNA-Seq data generated by Chromium 10X. Because the
359 *QRT2* data (Supplemental Table 3) include separate secession and residuum derived cells, we first
360 created an approximate composite AZ transcriptome by summing the counts per million for both
361 secession and residuum datasets with equal weighting. This dataset was full-transcript RNA-Seq, so we
362 estimated TPM using the formula below (Supplemental Table 4):

363
$$TPM_{geneX} = \frac{\frac{count_{geneX}}{length_{geneX}}}{\Sigma\left(\frac{count_{each_{gene}}}{length_{each_{gene}}}\right)} * 1{,}000{,}000$$

364 We then plotted the correlation value for each cluster on the previously generated UMAP embedding.

365 **Promoter cloning and reporter imaging**

366 Fragments ranging in size from 1 to 2.5 kilobases upstream of *MYB62*, *PECTIN LYASE-LIKE*, and *GDSL-*
367 *TYPE ESTERASE* were PCR amplified with PfuUltraII polymerase and cloned into pENTR (ThermoFisher),
368 then recombined into pMDC111[65] to create promoter::GFP fusions (primers are listed in Supplemental
369 Table 13). The *FAR5, IDA,* and *AT5G57785* upstream regions were PCR amplified by KAPA Hifi
370 polymerase (Roche) and cloned into an *Oryza sativa* H2B-VENUS fusion construct created by gene
371 synthesis (Twist Bioscience). The *H2B-VENUS* construct was first cloned into pENTR and recombined into
372 pGWB501[66]. This construct was created to include two AarI sites for Golden Gate cloning of promoter
373 fragments in one step (sequence in sup). The *AT5G57785pr::IDA* misexpression construct was
374 generated by cloning a synthetic *IDA* gene containing an upstream AarI cassette into pGWB501 [Twist
375 Biosciences]. This allowed us to directory clone the *AT5G57785* promoter fragment above into this
376 vector (sequence in sup). Primers are included in Supplemental Table 13. Siliques for the initial AZ
377 identification experiment were imaged on a Zeiss Axiozoom stereomicroscope with UV illumination. *IDA*
378 and *AT5G57785* reporter lines were images using a Zeiss LSM880 microscope with an EC Plan-Neofluar
379 10x/0.30 M27 objective. The lasers were 561nm and 488nm, with filters of 508-561nm and 570-670nm.
380 Beam splitter information is as follows: MBS: MBS 488/561, MBS_InVis:Plate, DBS1: Mirror. Each set of
381 images (residuum and secession AZs) were imaged from the same flower using the same settings.

382 **Non-Abscission zone Cell Annotation**

383 Clusters were defined by twice running the Seurat FindClusters function with both a low modularity
384 parameter (res = 2) and a high modularity parameter (res = 200), which results in clusters containing
385 hundreds/thousands of cells (broadly-resolved) and those having only tens of cells each (finely-
386 resolved), respectively. We then calculated expression z-scores of known marker genes [Supplemental
387 Table 14] in each cluster (both broadly and finely-resolved). These clusters were then annotated by
388 comparing the average marker gene z-scores. Cells that were annotated with the same cell identity in
389 broadly-resolved and finely-resolved clusters were considered confidently annotated. While those that
390 were not were labeled as "Unknown." This annotation approach combining results of complementary
391 modularity resolution was particularly useful for annotating rare cell-types while maintaining low noise
392 levels (Notebook 4).

393 **AZ pseudo-bulk DEG analysis comparing WT and *hae hsl2***

394 We performed pseudo-bulking for the AZ (Seurat cluster 11) for each WT and *hae hsl2* sample, yielding
395 four samples for each genotype (Notebook 5). We then used edgeR to normalize and calculate CPM and
396 LCPM matrices. We modeled whether the cells were sorted as a nuisance factor (to account for variation
397 due to FACS), and otherwise only included genotype as a factor (WT or mutant). We then constructed a
398 contrast testing the hypothesis that the genotype factor for the difference in expression between WT
399 and *hae hsl2* for each gene was equal to 0. The output of edgeR has been included as Supplemental
400 Table 7. A file with our edgeR functions has been included in Supplemental Code. This code requires an
401 Arabidopsis annotation file derived from TAIR10 included as Supplemental Table 15.

402 **GO term analysis**

403 For GO analysis we used shinyGO v 0.76[67]. For all analyses we displayed Biological Process terms at FDR
404 < .01. For GO analysis of WT AZs we used the output of the Seurat FindAllMarkers function to select
405 genes log2(Fold Enrichment) > 1 with FDR < .05 in the AZ. We used all genes from the FindAllMarkers
406 analysis as a universe (i.e., genes expressed in at least one cluster). For the WT-mutant DE GO analysis,
407 we took genes defined as DE log2(FC) > 1 with FDR < .05 with all genes expressed in at least 3 samples as
408 universe. GO analysis of the bulk DE/single-cell DE intersection was performed with a universe as the
409 genes defined to be expressed in the WT/*hae hsl2* pseudo-bulk DEG analysis.

410 **AZ subclustering**

411 AZ cells (those from cluster 11) were sub-divided into those of WT and *hae hsl2* origin, and each dataset
412 was reintegrated using a similar process as above (Notebook 6). We then performed coarse clustering
413 with resolution = .1 in Seurat which identified two transcriptionally distinct groups for both genotypes.
414 We performed pseudo-bulk Spearman correlation analysis comparing expression of each of the two
415 clusters in each genotype to previously published FACS secession and residuum datasets[15]. For
416 enrichment analysis we took the pseudo-bulked putative residuum cells and secession cells and
417 performed edgeR analysis as above, except we pooled the cells derived from the two FACS samples for
418 both mutant and WT due to a particularly low number of cells in WT sorted sample #1. The secession
419 and residuum associated genes are those with FDR < .05 and log2(fold enrichment) > 1 in the respective
420 cell types. We will note because the cells were clustered first before running the edgeR analysis, the
421 resulting gene lists were not unbiased estimates of differential expression. However, because we
422 performed identical procedures for WT and mutant, our Fisher's exact test is valid because it is testing
423 the hypothesis that the proportion of genes in this "enriched" set is different between the two
424 genotypes.

425 **Bulk RNA-Seq library generation and sequencing**

426 For the sorted *HAE-YFP* bulk samples, we sorted into 20 µl of RNA-Later then used the magnetic bead
427 based Direct-zol-96 MagBead RNA-Isolation kit (Zymo) to isolate RNA. For the protoplast test, we cut
428 three receptacles per replicate and digested as above. We harvested the tissue by spinning at 500 x g
429 and removing supernatant, leaving digested cells and undigested tissue in place, before freezing in liquid
430 N2. We simultaneously collected three receptacles per replicate in our unprotoplasted control where
431 tissue was placed in 10 µl of RNA-Later in the cap of a 1.7 ml microcentrifuge tube, tapped to the
432 bottom of the tube, immediately frozen in liquid N2, homogenized with a blue pestle, and performed
433 RNA isolation as above. We performed three replicates in each condition.

434 For the *fal-3/fal-7* bulk RNA-Seq experiment, we isolated receptacles from three stage 15 flowers for
435 each replicate of *er gl* (WT grandparent), *er gl hae-3 hsl2-3* (mutant parent), and *er gl hae-3 hsl2-3 fal-*
436 *3/fal-7* (suppressors). Tissue was placed into the cap of a 1.7 ml tube containing 10 µl RNA-Later. After
437 tapping the tissue to the bottom of the tube, we froze in liquid nitrogen. We then ground the tissue in
438 liquid N2 using blue pestles, and used the Zymo RNA-isolation kit as before. For all samples, RNA
439 integrity was checked with Bioanalyzer RNA Nano kit and quantified by Qubit.

440 For library generation, we used Lexogen Quantseq RNA-Seq using the manufacturer's protocol, with
441 instructions for "Low input" for the sorted samples due to input of only 5-10 ng total RNA input per
442 sample. We used the Unique Molecular Identifier (UMI) PCR add-on kit (Lexogen). Libraries were
443 indexed and sequenced on an Illumina NextSeq, High Output setting. Reads were aligned to the TAIR10

genome using the STAR aligner, deduplicated using UMI-Tools, and counted with HTSeq-Count. Counts were analyzed with edgeR. We defined "expressed genes" to be those with observed reads in three or more libraries. Raw reads have been deposited at the Sequence Read Archive under BioProject PRJNA857332.

PAGE analysis of abscission-associated gene expression in *fal* mutants

We constructed an expression matrix for the 67 bulk/single-cell intersection gene set for WT, *hae hsl2, hae hsl2 fal-3,* and *hae hsl2 fal-3* using the log2(CPM) values generated by edgeR (Notebooks 7 and 8). We then summed the log2(CPM) values of each gene for each sample and normalized to the average summed values of the *hae hsl2* samples before dividing by the number of genes in the analysis. The resulting quantity represents the average log2(FC) for each sample compared to the *hae hsl2* average. Last, we performed pairwise T-tests with Bonferroni Correction assuming equal variance.

Breakstrength measurements

The breakstrength of petals of stage 16 flowers (i.e., silique 1-2 mm above petals) in *er gl hae-3 hsl2-3* and *er gl hae-3 hsl2-3 fal-3/7* were measured using our previously described petal break strength meter and analysis script[45]. In brief, the petals were clamped to the meter and the flower pulled down with forceps until the petal detached. The maximum voltage was extracted from the output file of the meter. This voltage reading was converted to an equivalent force after calculation of a standard curve based on voltage readings of the meter attached to a varying number of objects of known weight (i.e., paper clips). For measurements taken at each temperature, we performed pairwise T-tests with Bonferroni Correction assuming equal variance.

***fal* mutant identification**

The *hae-3 hsl2-3* suppressor screen was performed as previously described[26]. For identification, we used TAIL-PCR[68] to amplify a PCR fragment in *fal-7* which was analyzed by Sanger sequencing. For *fal-3,* we used TAIL-PCR to identify an insertion in an exon of AT2G07690, which is a member of the Minichromosome Maintenance gene family involved in initiation of DNA replication. However, given the similar phenotype of *fal-7* we hypothesized there may exist an additional mutation in *MKP1*. We designed Sanger sequencing primers and tiled the coding sequence, detecting a G-> A SNP at bp 1357 in the *MKP1* coding sequence using primers listed in Supplemental Table 13. We performed linkage analysis in the *hae hsl2 x hae hsl2 fal-7* F2 population using genotyping primers listed in Supplemental Table 13.

Conflict of Interest

The authors declare they have no conflict of interest.

Funding

This work was supported by NSF MCB0743955 to JCW, NIH 1R35GM131725 to PNB, who is also supported by the Howard Hughes Medical Institute as an investigator, USDA 2021-67034-35139 to IWT, and Deutsche Forschungsgemeinschaft (DFG) 2403 to UO and CWH.

Acknowledgements

Figure 5I was created with BioRender.

482 1. Addicott, F. T. & Lynch, R. S. Physiology of abscission. *Annual Review of Plant Physiology* **6**, 211–238
483 (1955).
484 2. Taylor, J. E. & Whitelaw, C. A. Signals in abscission. *New Phytologist* **151**, 323–340 (2001).
485 3. Patharkar, O. R. & Walker, J. C. Connections between abscission, dehiscence, pathogen defense,
486 drought tolerance, and senescence. *Plant Science* **284**, 25–29 (2019).
487 4. Yu, Y. & Kellogg, E. A. Inflorescence abscission zones in grasses: diversity and genetic regulation.
488 *Annual Plant Reviews* **1**, 1–35 (2018).
489 5. Dutta, S. K., Gurung, G., Yadav, A., Laha, R. & Mishra, V. K. Factors associated with citrus fruit
490 abscission and management strategies developed so far: A review. *New Zealand Journal of Crop and*
491 *Horticultural Science* 1–22 (2022).
492 6. Kaur, R., Deol, J. & Dass, A. Physiology of abscission and crop regulation in cotton-a review. (2016).
493 7. Hossain, S., Kadkol, G., Raman, R., Salisbury, P. & Raman, H. Breeding Brassica napus for shatter
494 resistance. *In Plant Breeding* (2011).
495 8. Li, L.-F. & Olsen, K. To have and to hold: selection for seed and fruit retention during crop
496 domestication. *Current topics in developmental biology* **119**, 63–109 (2016).
497 9. Patharkar, O. R. & Walker, J. C. Advances in abscission signaling. *J Exp Bot* **69**, 733–740 (2018).
498 10. Meir, S. *et al.* Re-evaluation of the ethylene-dependent and-independent pathways in the
499 regulation of floral and organ abscission. *Journal of experimental botany* **70**, 1461–1467 (2019).
500 11. Ellis, C. M. *et al.* AUXIN RESPONSE FACTOR1 and AUXIN RESPONSE FACTOR2 regulate
501 senescence and floral organ abscission in Arabidopsis thaliana. *Development* **132**, 4563–4574 (2005).
502 12. Basu, M. M. *et al.* The manipulation of auxin in the abscission zone cells of Arabidopsis flowers
503 reveals that indoleacetic acid signaling is a prerequisite for organ shedding. *Plant physiology* **162**, 96–
504 106 (2013).

505 13. Kim, J. *et al.* New clothes for the jasmonic acid receptor COI1: delayed abscission, meristem
506 arrest and apical dominance. *PloS one* **8**, e60505 (2013).
507 14. Xu, P., Chen, H. & Cai, W. Transcription factor CDF4 promotes leaf senescence and floral organ
508 abscission by regulating abscisic acid and reactive oxygen species pathways in Arabidopsis. *EMBO*
509 *reports* **21**, e48967 (2020).
510 15. Lee, Y. *et al.* A lignin molecular brace controls precision processing of cell walls critical for
511 surface integrity in Arabidopsis. *Cell* **173**, 1468–1480 (2018).
512 16. Patterson, S. E. Cutting Loose. Abscission and Dehiscence in Arabidopsis. *Plant Physiology* **126**,
513 494–500 (2001).
514 17. Jinn, T. L., Stone, J. M. & Walker, J. C. HAESA, an Arabidopsis leucine-rich repeat receptor kinase,
515 controls floral organ abscission. *Genes Dev.* **14**, 108–117 (2000).
516 18. Cho, S. K. *et al.* Regulation of floral organ abscission in Arabidopsis thaliana. *Proc. Natl. Acad. Sci.*
517 *U.S.A.* **105**, 15629–15634 (2008).
518 19. Stenvik, G.-E. *et al.* The EPIP peptide of INFLORESCENCE DEFICIENT IN ABSCISSION is sufficient to
519 induce abscission in arabidopsis through the receptor-like kinases HAESA and HAESA-LIKE2. *Plant Cell*
520 **20**, 1805–1817 (2008).
521 20. Patharkar, O. R. & Walker, J. C. Floral organ abscission is regulated by a positive feedback loop.
522 *Proceedings of the National Academy of Sciences* 201423595 (2015).
523 21. Wang, Y., Wu, Y., Zhang, H., Wang, P. & Xia, Y. Arabidopsis MAPKK kinases YODA, MAPKKK3, and
524 MAPKKK5 are functionally redundant in development and immunity. *Plant Physiology* **190**, 206–210
525 (2022).
526 22. Schardon, K. *et al.* Precursor processing for plant peptide hormone maturation by subtilisin-like
527 serine proteinases. *Science* **354**, 1594–1597 (2016).

528 23. Butenko, M. A. *et al.* INFLORESCENCE DEFICIENT IN ABSCISSION controls floral organ abscission
529 in Arabidopsis and identifies a novel family of putative ligands in plants. *The Plant Cell Online* **15**,
530 2296–2307 (2003).
531 24. Santiago, J. *et al.* Mechanistic insight into a peptide hormone signaling complex mediating floral
532 organ abscission. *Elife* **5**, e15075 (2016).
533 25. Meng, X. *et al.* Ligand-induced receptor-like kinase complex regulates floral organ abscission in
534 Arabidopsis. *Cell reports* **14**, 1330–1338 (2016).
535 26. Taylor, I., Baer, J., Calcutt, R. & Walker, J. C. Hypermorphic SERK1 mutations function via a
536 SOBIR1 pathway to activate floral abscission signaling. *Plant physiology* **180**, 1219–1229 (2019).
537 27. Niederhuth, C. E., Patharkar, O. R. & Walker, J. C. Transcriptional profiling of the Arabidopsis
538 abscission mutant hae hsl2 by RNA-Seq. *BMC Genomics* **14**, 37 (2013).
539 28. Shi, C.-L. *et al.* Arabidopsis class I KNOTTED-like homeobox proteins act downstream in the IDA-
540 HAE/HSL2 floral abscission signaling pathway. *Plant Cell* **23**, 2553–2567 (2011).
541 29. Crick, J. *et al.* Floral organ abscission in Arabidopsis requires the combined activities of three
542 TALE homeodomain transcription factors. *Journal of Experimental Botany* **73**, 6150–6169 (2022).
543 30. Galindo-Trigo, S. *et al.* Dissection of the IDA promoter identifies WRKY transcription factors as
544 abscission regulators in Arabidopsis. *Journal of Experimental Botany* erae014 (2024).
545 31. Furuta, Y. *et al.* Petal abscission is promoted by jasmonic acid-induced autophagy at Arabidopsis
546 petal bases. *Nature Communications* **15**, 1098 (2024).
547 32. Ventimilla, D. *et al.* IDA (INFLORESCENCE DEFICIENT IN ABSCISSION)-like peptides and HAE
548 (HAESA)-like receptors regulate corolla abscission in Nicotiana benthamiana flowers. *BMC plant*
549 *biology* **21**, 1–14 (2021).
550 33. Estornell, L. H. *et al.* The IDA peptide controls abscission in Arabidopsis and Citrus. *Frontiers in*
551 *plant science* **6**, 1003 (2015).

552 34. Ying, P. *et al.* Identification and molecular characterization of an IDA-like gene from litchi,
553 LcIDL1, whose ectopic expression promotes floral organ abscission in Arabidopsis. *Scientific Reports*
554 **6**, 1–11 (2016).
555 35. Patharkar, O. R. & Walker, J. C. Core Mechanisms Regulating Developmentally Timed and
556 Environmentally Triggered Abscission. *Plant Physiol.* **172**, 510–520 (2016).
557 36. Patharkar, O. R., Gassmann, W. & Walker, J. C. Leaf shedding as an anti-bacterial defense in
558 Arabidopsis cauline leaves. *PLoS genetics* **13**, e1007132 (2017).
559 37. Fernandez, D. E. *et al.* The embryo MADS domain factor AGL15 acts postembryonically:
560 inhibition of perianth senescence and abscission via constitutive expression. *The Plant Cell* **12**, 183–
561 197 (2000).
562 38. Chen, M.-K. *et al.* The MADS box gene, FOREVER YOUNG FLOWER, acts as a repressor controlling
563 floral organ senescence and abscission in Arabidopsis. *The Plant Journal* **68**, 168–185 (2011).
564 39. Chen, W.-H. *et al.* Regulatory network for FOREVER YOUNG FLOWER-like genes in regulating
565 Arabidopsis flower senescence and abscission. *Communications Biology* **5**, 662 (2022).
566 40. Stuart, T. *et al.* Comprehensive integration of single-cell data. *Cell* **177**, 1888–1902 (2019).
567 41. Zhou, Y. *et al.* Genetic control of seed shattering in rice by the APETALA2 transcription factor
568 SHATTERING ABORTION1. *The Plant Cell* **24**, 1034–1048 (2012).
569 42. Zhang, T.-Q., Chen, Y. & Wang, J.-W. A single-cell analysis of the Arabidopsis vegetative shoot
570 apex. *Developmental Cell* **56**, 1056–1074 (2021).
571 43. Klepikova, A. V., Kasianov, A. S., Gerasimov, E. S., Logacheva, M. D. & Penin, A. A. A high
572 resolution map of the Arabidopsis thaliana developmental transcriptome based on RNA-seq profiling.
573 *The Plant Journal* **88**, 1058–1070 (2016).
574 44. Robinson, M. D., McCarthy, D. J. & Smyth, G. K. edgeR: a Bioconductor package for differential
575 expression analysis of digital gene expression data. *Bioinformatics* **26**, 139–140 (2010).

576 45. Lease, K. A., Cho, S. K. & Walker, J. C. A petal breakstrength meter for Arabidopsis abscission
577 studies. *Plant Methods* **2**, 2 (2006).
578 46. Kim, S.-Y. & Volsky, D. J. PAGE: Parametric Analysis of Gene Set Enrichment. *BMC Bioinformatics*
579 **6**, 144 (2005).
580 47. Ulm, R. *et al.* Distinct regulation of salinity and genotoxic stress responses by Arabidopsis MAP
581 kinase phosphatase 1. *The EMBO Journal* **21**, 6483–6493 (2002).
582 48. Bartels, S. *et al.* MAP kinase phosphatase1 and protein tyrosine phosphatase1 are repressors of
583 salicylic acid synthesis and SNC1-mediated responses in Arabidopsis. *The Plant Cell* **21**, 2884–2897
584 (2009).
585 49. Sexton, R. & Roberts, J. A. Cell biology of abscission. *Annual Review of Plant Physiology* **33**, 133–
586 162 (1982).
587 50. Taylor, I. *et al.* Analysis of Phosphorylation of the Receptor-Like Protein Kinase HAESA during
588 Arabidopsis Floral Abscission. *PLoS ONE* **11**, e0147203 (2016).
589 51. Friedel, R. *Edison's Electric Light*. (Rutgers University Press, 1986).
590 52. Niederhuth, C. E., Cho, S. K., Seitz, K. & Walker, J. C. Letting Go is Never Easy: Abscission and
591 Receptor-Like Protein Kinases. *Journal of integrative plant biology* **55**, 1251–1263 (2013).
592 53. Taylor, I. & Walker, J. C. Transcriptomic evidence for distinct mechanisms underlying abscission
593 deficiency in the Arabidopsis mutants haesa/haesa-like 2 and nevershed. *BMC Research Notes* **11**,
594 754 (2018).
595 54. Evrard, A. *et al.* Fluorescence-activated cell sorting for analysis of cell type-specific responses to
596 salinity stress in Arabidopsis and rice. in *Plant Salt Tolerance* 265–276 (Springer, 2012).
597 55. Tan, C. K. *et al.* Functional characterization of RNA-dependent DNA polymerase and RNase H
598 activities of a recombinant HIV reverse transcriptase. *Biochemistry* **30**, 2651–2655 (1991).

599 56. Denyer, T. & Timmermans, M. C. Crafting a blueprint for single-cell RNA sequencing. *Trends in*
600 *Plant Science* (2021).
601 57. Shahan, R. *et al.* A single-cell Arabidopsis root atlas reveals developmental trajectories in wild-
602 type and cell identity mutants. *Developmental cell* **57**, 543–560 (2022).
603 58. Bray, N. L., Pimentel, H., Melsted, P. & Pachter, L. Near-optimal probabilistic RNA-seq
604 quantification. *Nature biotechnology* **34**, 525–527 (2016).
605 59. Melsted, P., Ntranos, V. & Pachter, L. The barcode, UMI, set format and BUStools. *Bioinformatics*
606 **35**, 4472–4473 (2019).
607 60. Moses, L. & Pachter, L. BUSpaRse: kallisto| bustools R utilities. *R package version* **1**, (2019).
608 61. Pagès, H. BSgenome: Software infrastructure for efficient representation of full genomes and
609 their SNPs. *R package version 1.64.0, https://bioconductor.org/packages/BSgenome* (2020).
610 62. Kawahara, Y. *et al.* Improvement of the Oryza sativa Nipponbare reference genome using next
611 generation sequence and optical map data. *Rice* **6**, 1–10 (2013).
612 63. Lun, A. T., Riesenfeld, S., Andrews, T., Gomes, T. & Marioni, J. C. EmptyDrops: distinguishing cells
613 from empty droplets in droplet-based single-cell RNA sequencing data. *Genome biology* **20**, 1–9
614 (2019).
615 64. McGinnis, C. S., Murrow, L. M. & Gartner, Z. J. DoubletFinder: doublet detection in single-cell
616 RNA sequencing data using artificial nearest neighbors. *Cell systems* **8**, 329–337 (2019).
617 65. Curtis, M. D. & Grossniklaus, U. A gateway cloning vector set for high-throughput functional
618 analysis of genes in planta. *Plant physiology* **133**, 462–469 (2003).
619 66. Nakagawa, T. *et al.* Development of series of gateway binary vectors, pGWBs, for realizing
620 efficient construction of fusion genes for plant transformation. *Journal of bioscience and*
621 *bioengineering* **104**, 34–41 (2007).

622 67. Ge, S. X., Jung, D. & Yao, R. ShinyGO: a graphical gene-set enrichment tool for animals and
623 plants. *Bioinformatics* **36**, 2628–2629 (2020).
624 68. Liu, Y.-G., Mitsukawa, N., Oosumi, T. & Whittier, R. F. Efficient isolation and mapping of
625 Arabidopsis thaliana T-DNA insert junctions by thermal asymmetric interlaced PCR. *The Plant Journal*
626 **8**, 457–463 (1995).
627

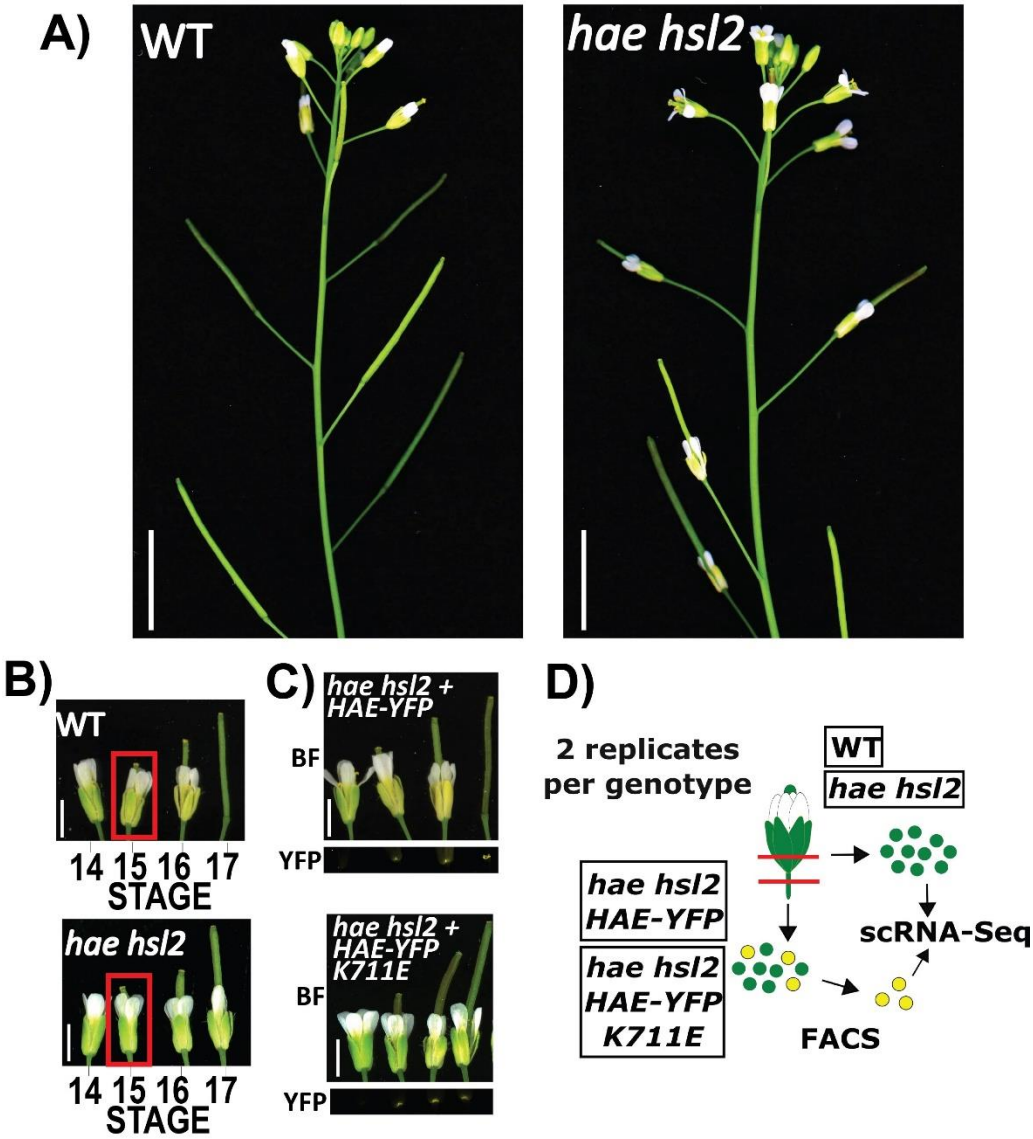

Figure 1: Background and experimental system

A) Floral abscission phenotype of WT and *hae hsl2* mutant. Scale bar = 10 mm.
B) Flower stages in WT and *hae hsl2* mutant. Scale bar = 2 mm.
C) Phenotype of transgenic *hae hsl2* expressing wild-type *HAEpr::HAE-YFP* and *HAEpr::HAE-YFP K711E* (bright-field/BF and YFP). Scale bar = 2 mm.
D) Diagram of AZ single-cell isolation and experimental procedure.

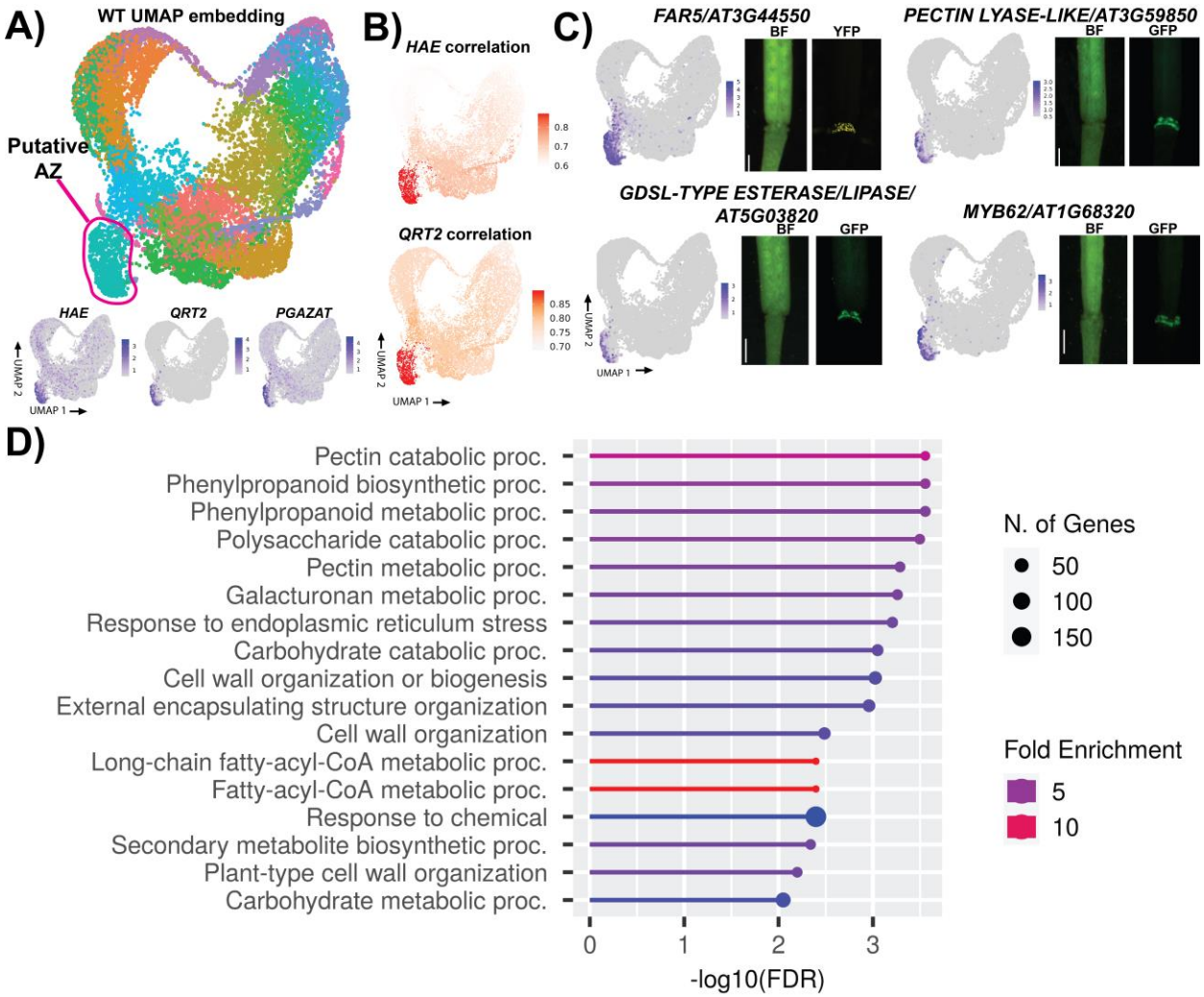

Figure 2: Identification and characterization of AZ cells by single-cell RNA-Sequencing

A) UMAP embedding of WT cells with putative AZ cluster circles in pink (top) and expression of AZ marker genes on UMAP (bottom). Expression is on Seurat SCT scale.
B) Cluster-wise pseudo-bulk Spearman correlation with sorted bulk data of *HAEpr::HAE-YFP* (top) or *QRT2pr::GFP* (bottom).
C) Expression of 4 putative AZ marker genes in single-cell UMAP embedding and in the young siliques of *promoter::fluorescent protein* expressing transgenic plants (bright-field/BF and YFP or GFP). Expression is on Seurat SCT scale. Scale bar = .7 mm.
D) Gene Ontology Biological Process term enrichment of AZ specific genes.

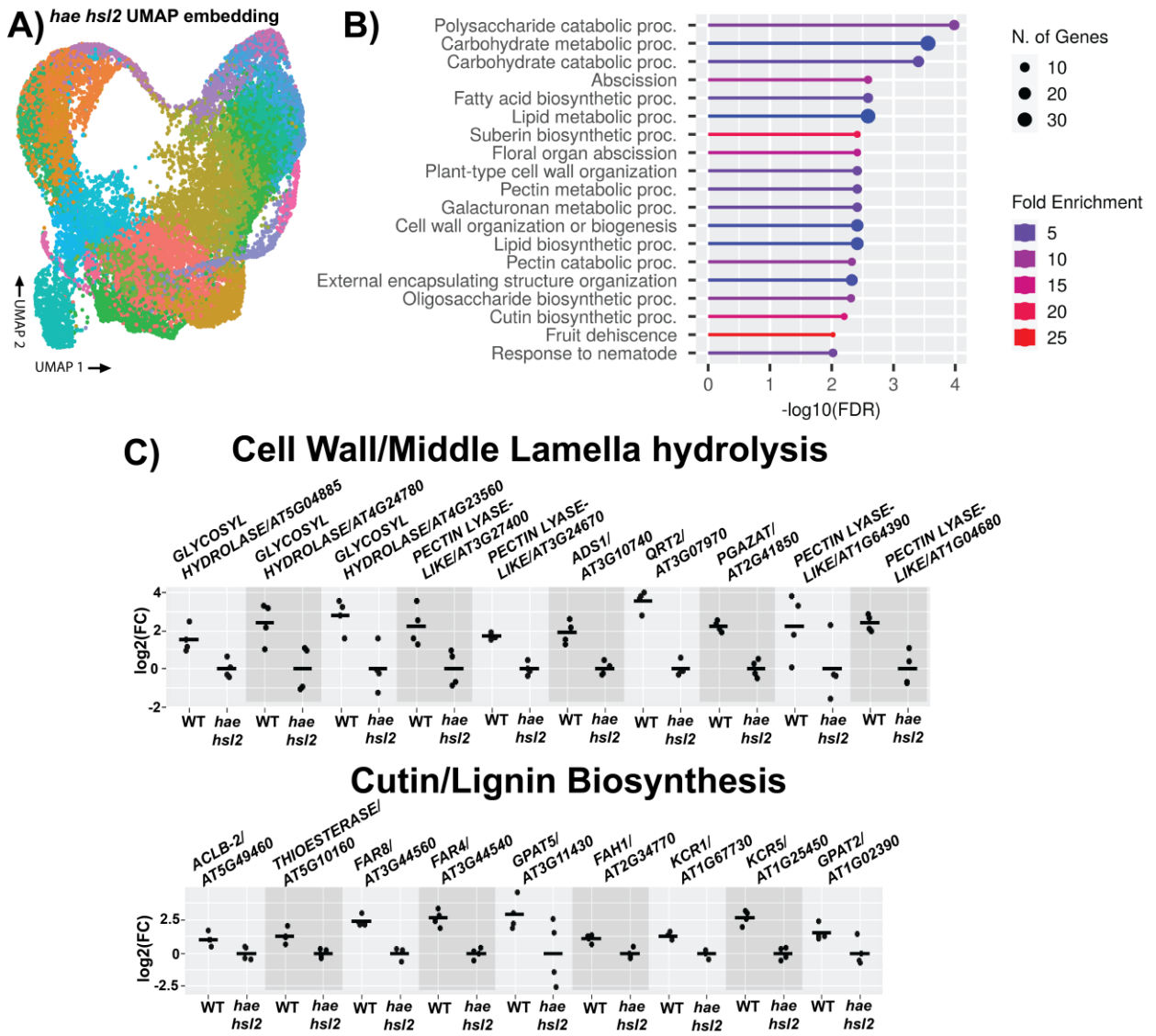

<u>Figure 3: Analysis of differentially expressed genes in the *hae hsl2* mutant AZ</u>

A) UMAP embedding of *hae hsl2* cells.

B) Gene Ontology Biological Process term enrichment of DE genes higher in WT (FDR <.05, log2(FC) > 1).

C) Expression of cell wall/middle lamella hydrolysis genes (top) and cutin/lignin biosynthesis genes (bottom). Scale is log2(FC) for each sample relative to the average of *hae hsl2*. All genes are lower in mutant with FDR < .05.

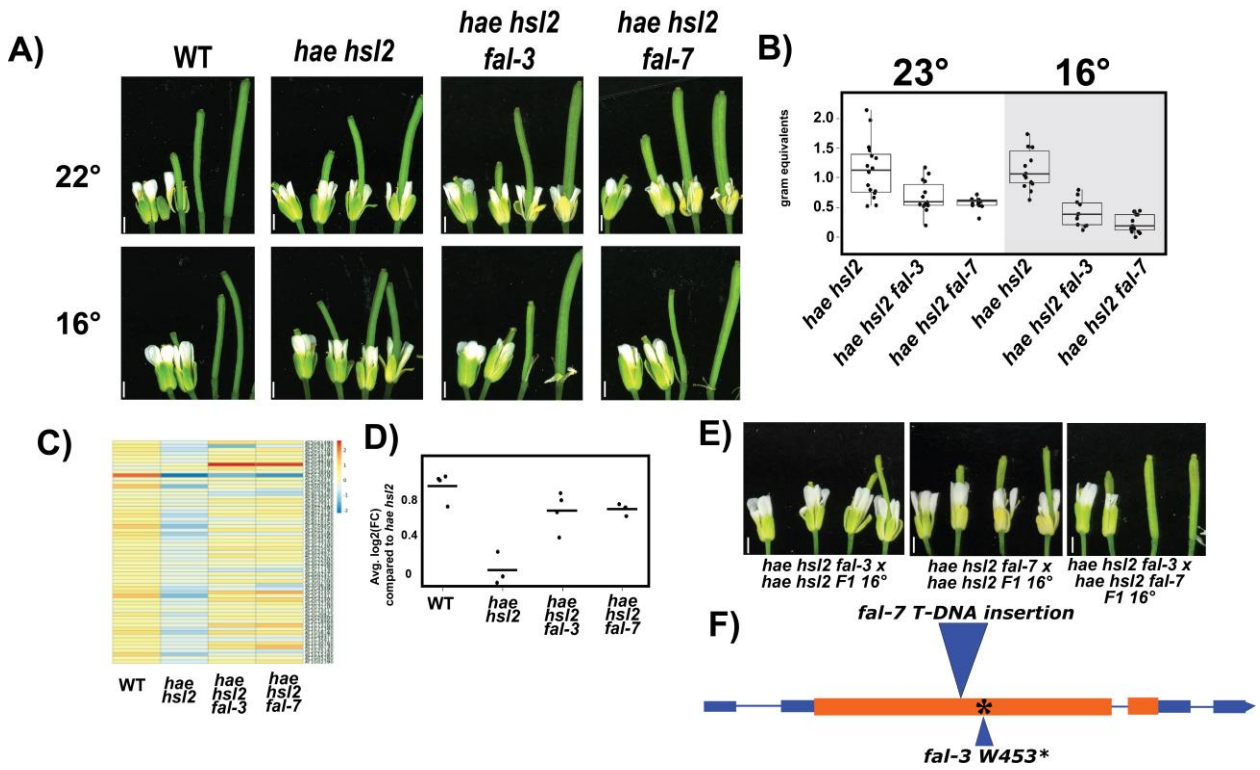

Figure 4: Analysis and identification of *hae hsl2* suppressors

A) Phenotypes of WT, *hae hsl2, hae hsl2 fal-3,* and *hae hsl2 fal-7* at 22° (left) or 16° (right). Siliques were gently tapped to remove remnant floral organs. Scale bar = 1 mm.
B) Breakstrength phenotypes of *hae hsl2, hae hsl2 fal-3,* and *hae hsl2 fal-7* at 23° (left) or 16° (right).
C) Heatmap of expression values for 67 genes identified as higher in WT in both bulk and single-cell DE analysis comparing WT to *hae hsl2.* Values are log2(FC) compared the overall average expression across all genotypes.
D) Average log2(FC) comparing each sample to the average of *hae hsl2* for the genes in part C.
E) Complementation crosses of *fal* mutants. Scale bar = 1 mm.
F) Gene model of *MKP1* depicting mutations in *fal-3* and *fal-7.* Orange colors represent exons, blue represent UTRs, and thin lines represent introns.

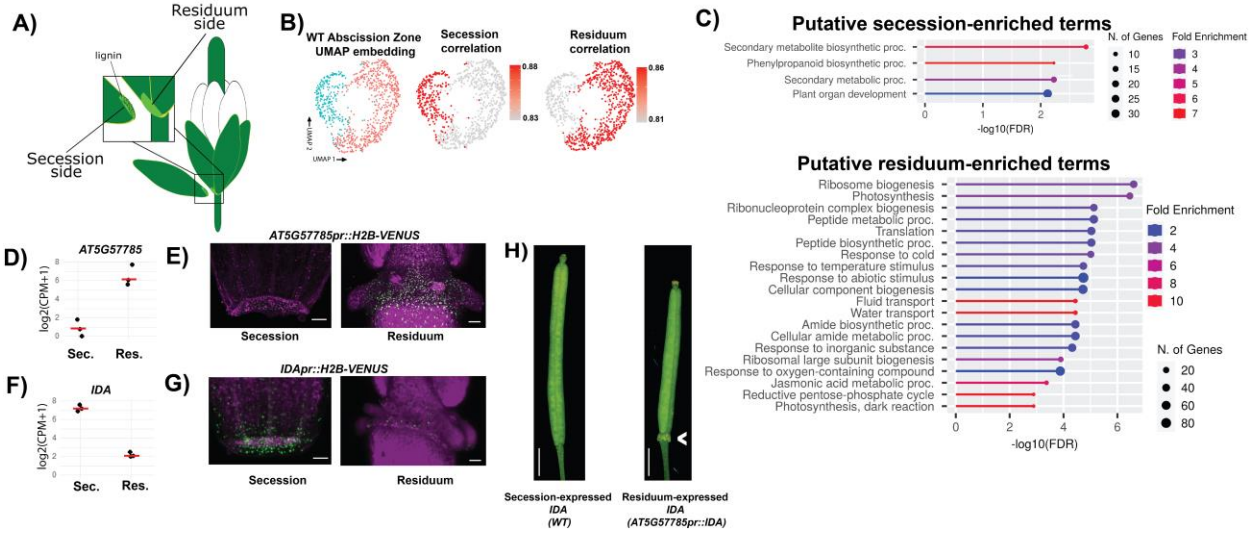

Figure 5: Spatial analysis of the AZ

A) Schematic view of the spatial organization of the AZ.
B) Low resolution Louvain clustering and UMAP embedding of WT AZ cells (left) and Spearman correlation with sorted bulk secession data (middle) or residuum data (right).
C) GO Term enrichment of genes differentially enriched in the putative secession cells (top panel) or putative residuum cells (bottom panel).
D) Pseudobulk log2(CPM + 1) of *AT5G57785* in putative secession ("sec.") and residuum ("res.") cells.
E) *AT5G57785pr::H2B-VENUS* expression in secession and residuum cells.
F) Pseudobulk log2(CPM + 1) of *IDA* in putative secession and residuum cells.
G) *IDApr::H2B-VENUS* expression in secession and residuum cells
H) *IDA* expression phenotype in WT (left) and residuum specific *AT5G57785pr::IDA* misexpression phenotype (right).
I) Low resolution Louvain clustering and UMAP embedding of *hae hsl2* AZ cells (left) and Spearman

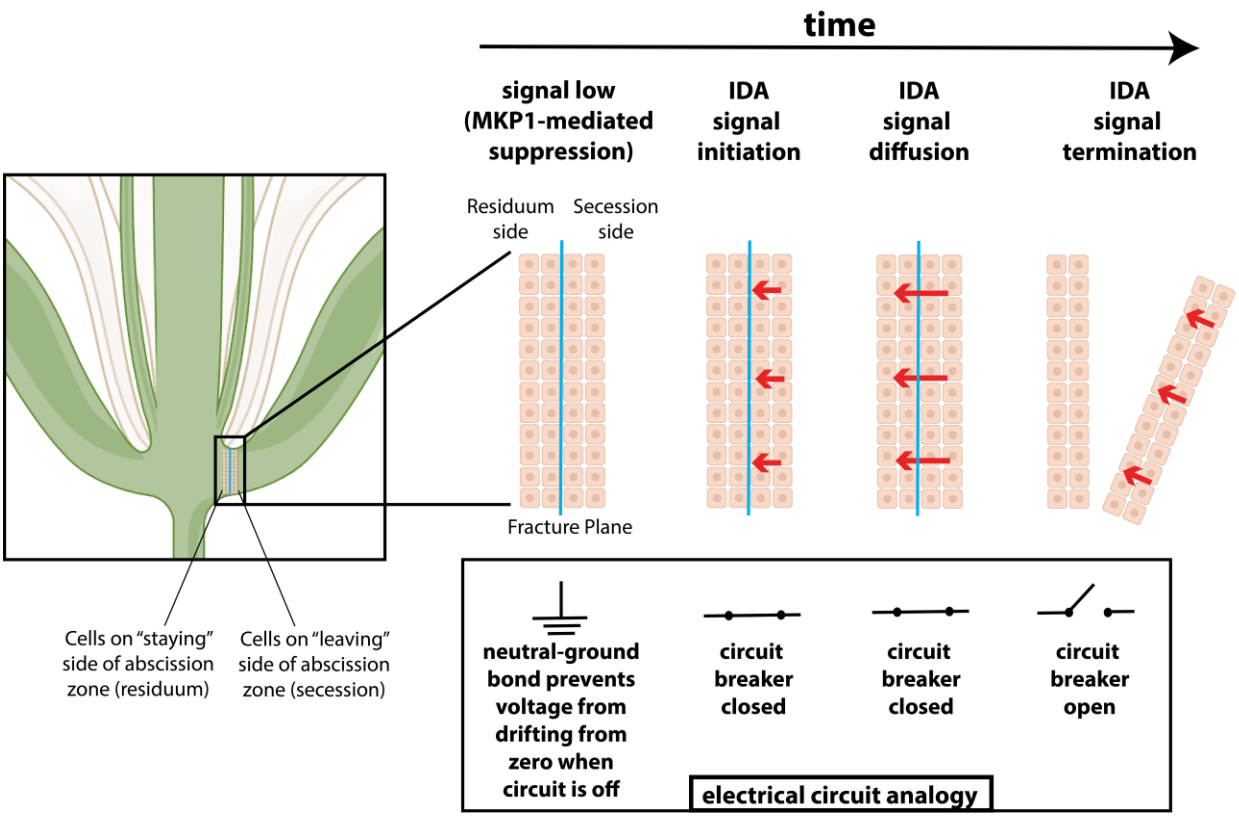

Figure 6: Diagram depicting the molecular signaling circuit controlling abscission signal initiation and termination.

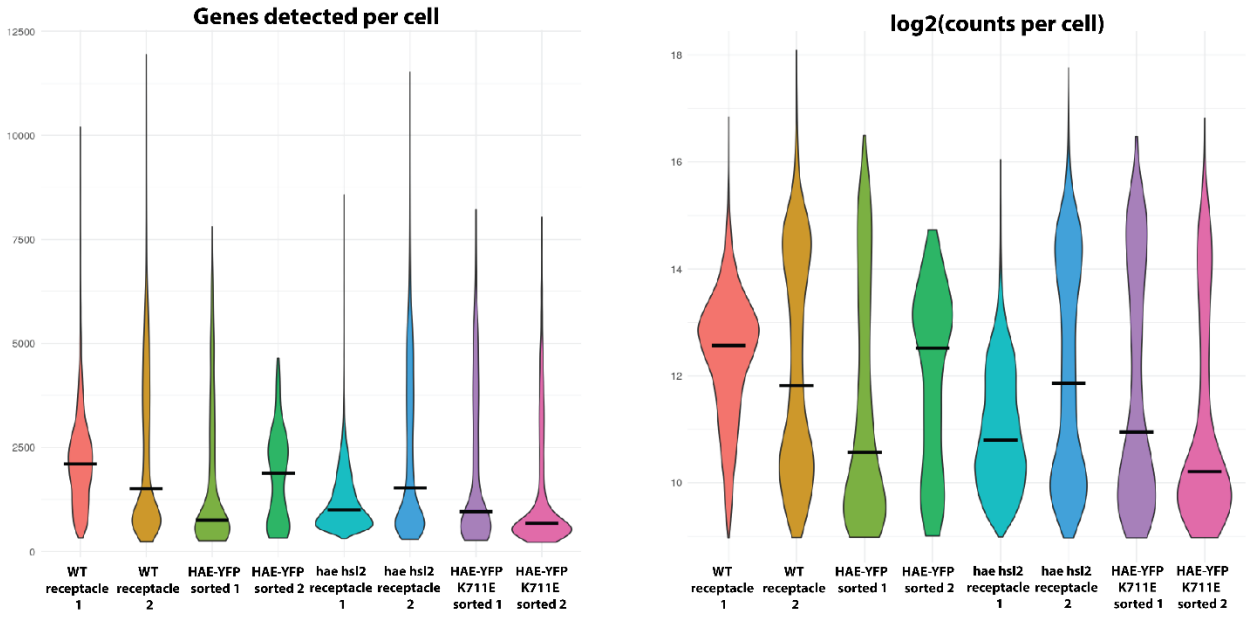

Supplemental Figure 1: Plots of the number of genes detected per cell and log2(counts per cell)

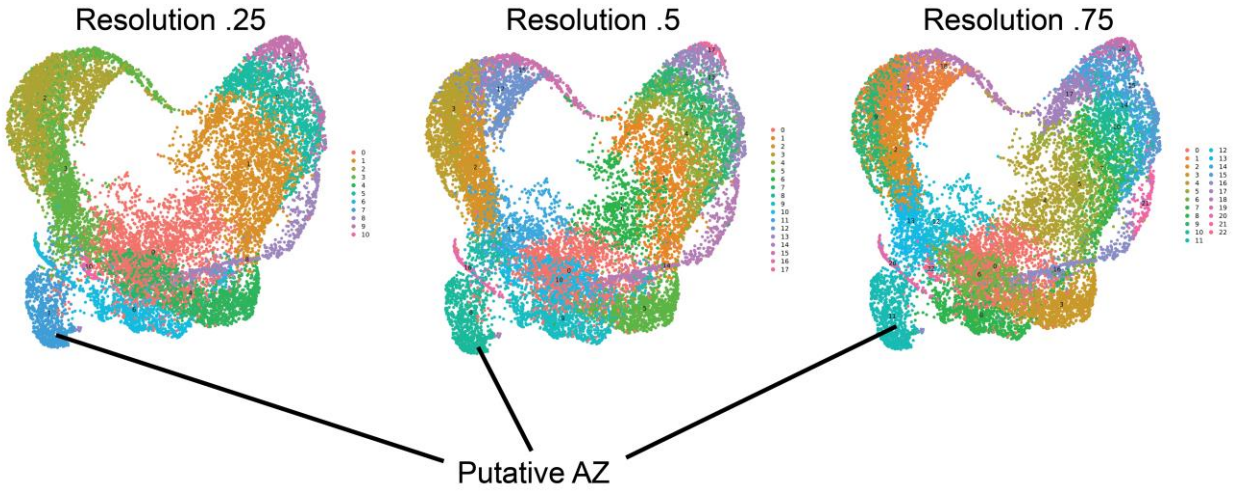

Supplemental Figure 2: The putative AZ cluster is similar across a range of clustering resolutions

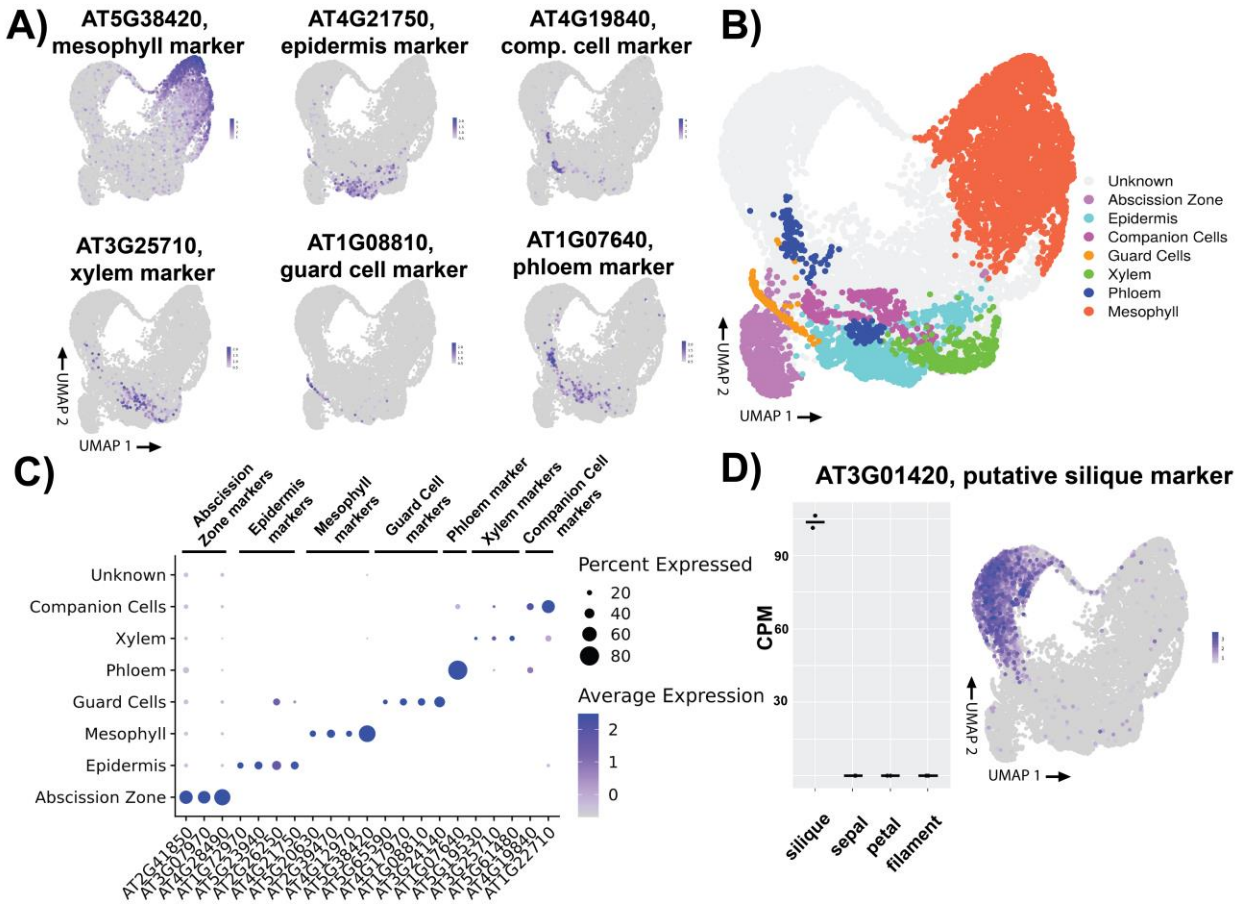

<u>Supplemental Figure 3</u>: Identification of additional cell types

A) Plotting cell type markers identified from a prior single-cell study of Arabidopsis leaves.
B) Tentative cell-type identification based on expression of known marker cell-type marker genes.
C) Distribution of marker gene expression across putative cell types.
D) Expression of putative silique marker gene in previously published bulk data (left panel), and expression of the same putative silique marker gene from our single-cell data (right panel).

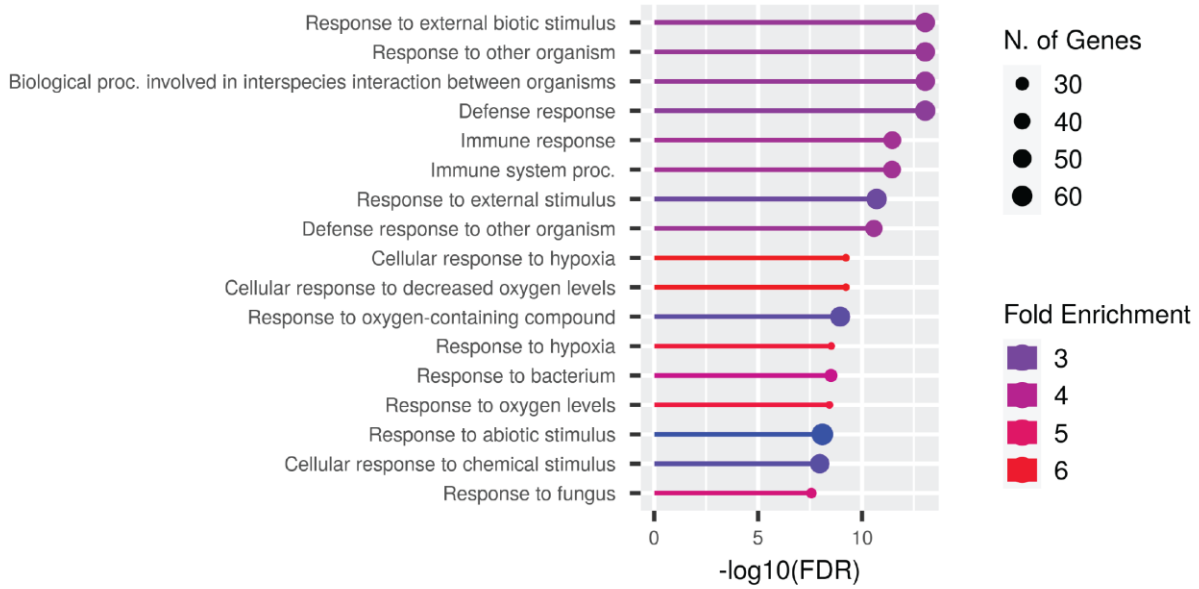

<u>Supplemental Figure 4:</u> GO term enrichment analysis of genes higher in *hae hsl2* compared to WT AZs.

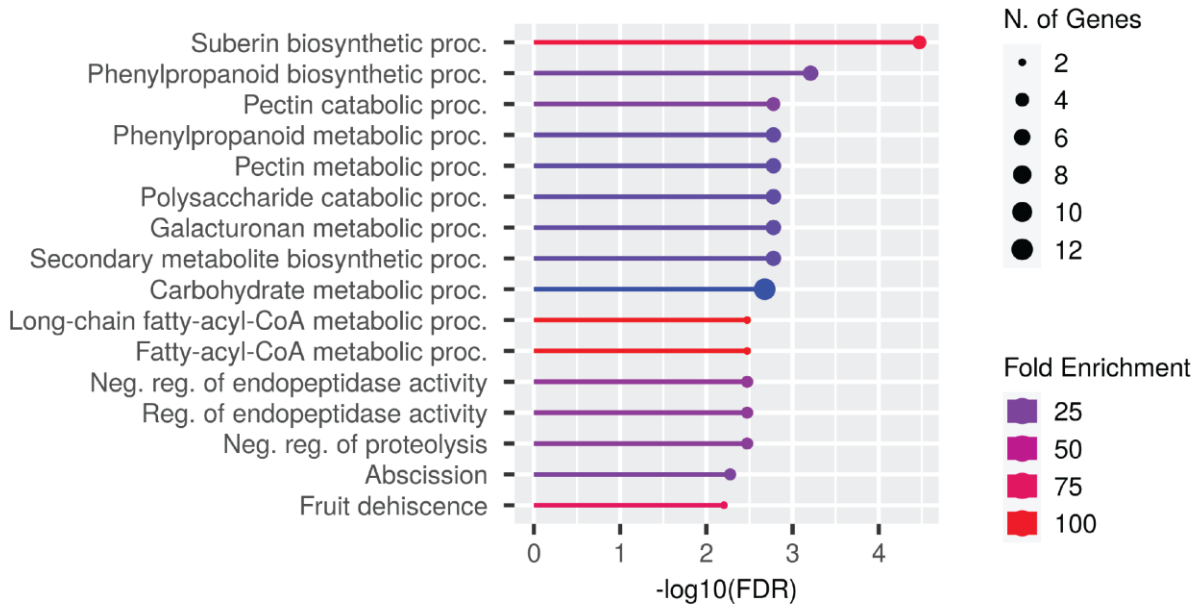

<u>Supplemental Figure 5:</u> GO term enrichment analysis of genes lower in *hae hsl2* compared to WT from both bulk and single-cell RNA-Seq.

genotype	*+/+*	*+/fal-7*	*fal-7/fal-7*
suppression phenotype	0/8	0/34	18/18

<u>Supplemental Figure 6:</u> Association of phenotype and genotype in an F2 *hae hsl2 x hae hsl2 fal-7* backcross population.

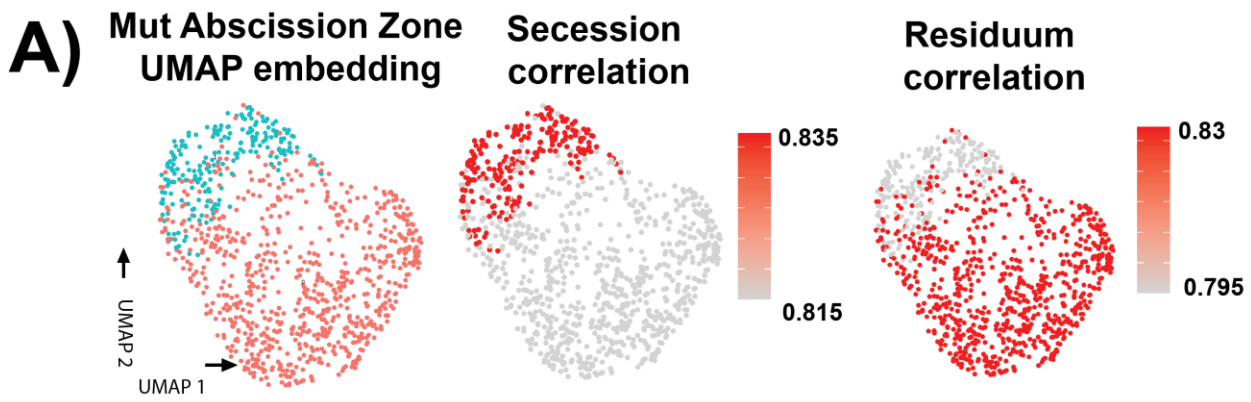

B)

	Secession-associated genes	Residuum-associated genes	Total genes
WT	306	540	846
hae hsl2	178	196	374

<u>Supplemental Figure 7</u>: Sub-clustering and differential enrichment analysis of mutant AZ cells

A) UMAP and coloration of low-resolution mutant AZ cell clusters (left), along with correlation to bulk secession and residuum RNA-Seq data (right)
B) Table of differentially enriched genes in secession and residuum cells across both WT and mutant samples

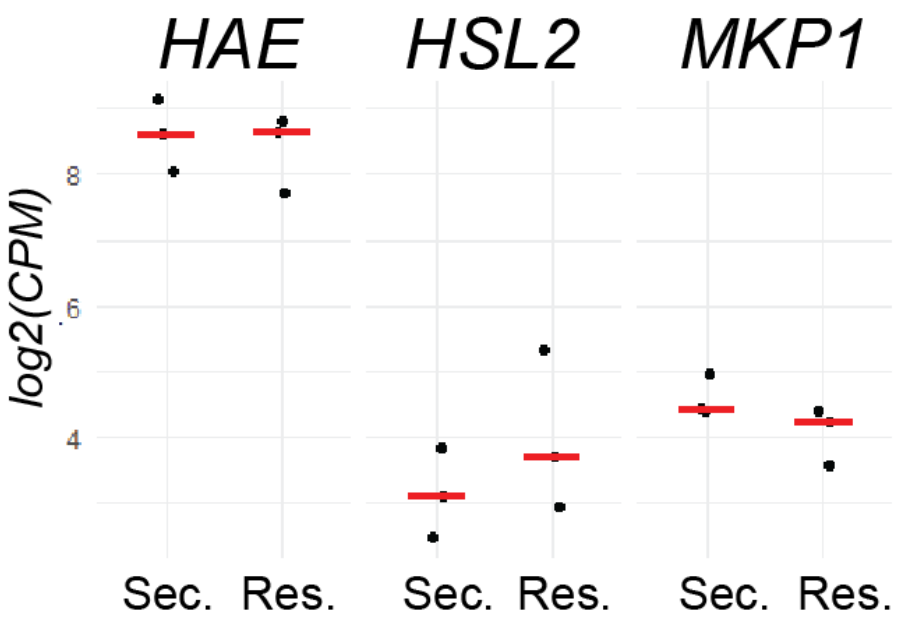

<u>Supplemental Figure 8:</u> Pseudobulk log2(CPM) of *HAE, HSL2,* and *MKP1* in putative secession and residuum cells.

Supplemental Table Legends

Supplemental Table 1- Median UMIs, Median genes detected, and number of cells called per sample.

Supplemental Table 2- Average and replicate-specific transcripts per million (TPMs) for 3 replicate samples of FACS sorted *HAE-YFP* YFP+ cells.

Supplemental Table 3- Lee et al data. Average and replicate-specific counts per million (CPMs) for 3 replicate samples of FACS sorted *QRT2-YFP* YFP+ cells for both residuum and secession cells.

Supplemental Table 4- Lee et al data. pseudoTPM for the average *QRT2-YFP* YFP+ cells for both residuum and secession cells. All other data in this study is 3' sequencing and intrinsically TPM. We transformed the full-length transcript measurements of Lee et al to pseudo-TPM using the formula in Materials and Methods. This puts the data on a similar scale for purposes of calculating correlation, etc.

Supplemental Table 5- Output of Seurat FindMarkers function reporting differentially enriched genes from the WT putative abscission zone cluster ("cluster 11") compared to all other cells in the WT samples. "pct.1" represents the percentage of cells in cluster 11 where each gene was detected, and "pct.2" is the percentage of cells outside cluster 11 where each gene was detected.

Supplemental Table 6- All genes detected in at least one cluster in the single-cell data, used for Gene Ontology analysis.

Supplemental Table 7- edgeR analysis of pseudo-bulk data comparing WT and mutant samples.

Supplemental Table 8- Intersection of genes determined to be statistically significantly higher in WT compared to mutant in the pseudo-bulk single-cell analysis and prior receptacle bulk analysis.

Supplemental Table 9- TPMs of Columbia, *hae-3 hsl2-3, hae-3 hsl2-3 fal-3, hae-3 hsl2-3 fal-7* bulk RNA-Seq.

Supplemental Table 10- edgeR output of pseudo-bulk differential enrichment analysis comparing putative secession and residuum cells in WT.

Supplemental Table 11- edgeR output of pseudo-bulk differential enrichment analysis comparing putative secession and residuum cells in mutant.

Supplemental Table 12- edgeR output of receptacle protoplasting experiment. Receptacles were either dissected and directly frozen in N2 or subjected to the protoplasting procedure before harvesting all cells and tissue before RNA preparation.

Supplemental Table 13- Primers for cloning, genotyping, and sequencing.

Supplemental Table 14- Marker genes for known shoot-tissue cell types.

Supplemental Table 15- Gene annotations used in all gene lists.